Mitochondrial protein heterogeneity stems from the stochastic nature of co-translational protein targeting in cell senescence

Abdul Haseeb Khan [1], Xuefang Gu [1], Rutvik J. Patel[2], Prabha Chuphal[2], Matheus P. Viana[3], Aidan I. Brown[2], Brian M. Zid [4] & Tatsuhisa Tsuboi [1,4,5]

A decline in mitochondrial function is a hallmark of aging and neurodegenerative diseases. It has been proposed that changes in mitochondrial morphology, including fragmentation of the tubular mitochondrial network, can lead to mitochondrial dysfunction, yet the mechanism of this loss of function is unclear. Most proteins contained within mitochondria are nuclear-encoded and must be properly targeted to the mitochondria. Here, we report that sustained mRNA localization and co-translational protein delivery leads to a heterogeneous protein distribution across fragmented mitochondria. We find that age-induced mitochondrial fragmentation drives a substantial increase in protein expression noise across fragments. Using a translational kinetic and molecular diffusion model, we find that protein expression noise is explained by the nature of stochastic compartmentalization and that co-translational protein delivery is the main contributor to increased heterogeneity. We observed that cells primarily reduce the variability in protein distribution by utilizing mitochondrial fission-fusion processes rather than relying on the mitophagy pathway. Furthermore, we are able to reduce the heterogeneity of the protein distribution by inhibiting co-translational protein targeting. This research lays the framework for a better understanding of the detrimental impact of mitochondrial fragmentation on the physiology of cells in aging and disease.

Mitochondria are hubs for metabolites and energy generation and have been deemed important for age-related processes and diseases, including cancer and neurodegeneration[1–3]. The loss of mitochondrial function in these pathological phenotypes is tied to cell-to-cell variability in gene expression caused by the amount and functional mitochondrial heterogeneity within a cell[4–6]. Two different aspects of

mitochondrial heterogeneity of a single cell are often discussed: genetic heterogeneity and functional heterogeneity[7]. Genetic heterogeneity is based on the distribution of mtDNA and varying rates of mtDNA gene transcription and translation, which increase the heterogeneity of protein levels for each fragment[8], known as noise[9]. On the other hand, definitions of functional heterogeneity are more

[1]Institute of Biopharmaceutical and Health Engineering, Tsinghua Shenzhen International Graduate School, Shenzhen 518055, China. [2]Department of Physics, Toronto Metropolitan University, Toronto, ON M5B 2K3, Canada. [3]Allen Institute for Cell Science, Seattle, WA 98109, USA. [4]Department of Chemistry and Biochemistry, University of California San Diego, La Jolla, CA 92093, USA. [5]Tsinghua-SIGS & Jilin Fuyuan Guan Food Group Joint Research Center, Tsinghua Shenzhen International Graduate School, Shenzhen 518055, China. ✉e-mail: zid@ucsd.edu; ttsuboi@sz.tsinghua.edu.cn

diverse, involving cristae structure[10–12], membrane potential[13,14], and pH[15,16] distributions in mitochondria. Both genetic and functional heterogeneities are influenced by mitochondrial morphology, especially by fragmentation. The sustained fragmentation of mitochondria precludes the exchange of mitochondrial contents among mitochondria, leading to non-optimal protein stoichiometry of mitochondrial complexes, disruption of normal protein homeostasis, and loss of functional mitochondria[17–24]. While fragmented mitochondria are suggested to be degraded by the mitochondria quality control pathway through mitophagy[25], hyper-fragmented mitochondria, which is also a phenotypic feature of diseases, require more dynamic regulatory mechanisms to eliminate the potentially harmful mitochondrial state from the cells, such as mitochondrial fission-fusion reactions and tubular structure formation[26].

Mitochondrial proteins are encoded mainly in the nuclear genome and then imported to mitochondria from the cytoplasm[27]. A large fraction of mitochondrial protein-coding mRNA is localized to the mitochondrial outer membrane and co-translationally imports proteins into mitochondria[28–34]. The mechanism of mRNA localization is based on both the 3′ UTR and coding regions, primarily through mitochondrial targeting sequences (MTSs)[29,32–36]. While there is an advancing understanding of mitochondrial mRNA localization mechanisms, the impact of co-translational protein targeting on mitochondrial function under different mitochondrial morphologies is poorly understood. Furthermore, mtDNA only encodes a small number of genes, eight protein-coding genes in *Saccharomyces cerevisiae*[37], raising the question of whether the distribution of nuclear-encoded proteins, which are imported into mitochondria from the cytoplasm, causes mitochondrial dysfunction. Here, we report that co-translational protein delivery and mitochondrial fragmentation together lead to heterogeneity in protein distribution to mitochondria in aged cells. Our work shows that mitochondrial fragmentation affects protein targeting and results in higher protein heterogeneity in each mitochondrial fragment. This heterogeneity is typically homogenized by the mitochondrial fission-fusion processes, not the mitophagy pathway. By inhibiting the co-translational protein delivery, we successfully reduced protein heterogeneity. We propose that age-associated fragmentation of mitochondria induces an increased heterogeneity of mitochondrial proteins, ultimately leading to accelerated cell senescence.

Results

Aging increases heterogeneity in mitochondrial protein distribution in each mitochondrion

Nuclear-encoded mitochondrial protein import is essential for the proper functioning of mitochondria. Disruption of this process has been linked to a number of diseases[38]. The core of the TIM23 complex, composed of Tim23p, Tim50p, and Tim17p, forms a translocase of the inner mitochondrial membrane that is important for importing a large number of matrix proteins[39]. To analyze the effect of aging on the distribution of mitochondrial proteins in yeast, we adopted mother-enrichment-program (MEP) yeast strains[40], with which we can continuously observe mother cells by inhibiting a cell cycle progression of the daughter cell and then determined the protein expression levels of Tim50p and Tim23p by quantitative microscopic techniques. We analyzed cells at 0 divisions (0 h) and ~16 divisions (24 h) following the induction of MEP (Fig. 1A, Supplementary Fig. 1). Consistent with prior research[24], the number of fragments increased with aging (24 h) (Fig. 1B). To evaluate the mitochondrial fragmentation in each cell, we calculated the proportion that each mitochondrion in a cell contributes to the total mitochondrial volume at the single-cell level. For a cell with a single, fully tubular mitochondrion, this portion would be 1; whereas, for a cell with many highly fragmented mitochondria, the portion for each mitochondrion would be much smaller than 1, as the volume of each fragment only contributes a small fraction of the total mitochondrial volume. At 24 h, when there are many fragments per

cell, we see that the typical portion of mitochondria for each mitochondrion is small, while a much larger portion for each mitochondrion was observed at 0 h (Fig. 1C). Imbalances in protein stoichiometry can lead to the loss of protein complex function and even protein aggregation-driving proteotoxic stress[41]. As each fragmented mitochondria can act as an independent fundamental unit, we sought to quantify the heterogeneity of Tim50 and Tim23 proteins across mitochondrial fragments. We observed more significant heterogeneity in the Tim50/Tim23 relative protein expression in each mitochondrial fragment (Fig. 1D) and confirmed the significant increase in the noise (coefficient of variation) level with increased age (Fig. 1E). We hypothesized that the age-induced changes in mitochondrial morphology may contribute to this increased noise level, so we analyzed the relationship between the protein expression level and mitochondrial fragment size. The increased number of smaller mitochondrial fragments during aging was linked to the increased heterogeneity of the Tim50/Tim23 relative protein levels (Fig. 1F, G). Interestingly, the overall protein expression of the fragments remained constant, as the linear regression line of Tim50/Tim23 relative protein level in Fig. 1F stayed the same over the fragments. These results provide a de novo observation that aging increases heterogeneity in the distribution of mitochondrial protein at the overall fragment level.

Stochastic nature of co-translational proteins targeting increased protein heterogeneity

Our observation suggests that small portion sizes of mitochondria cause high heterogeneity in protein expression, leading to increased protein expression heterogeneity in aged cells with predominantly small mitochondria. Most mitochondrial proteins are imported from the cytoplasm; however, the mRNA number in a single cell is limited to 5-10 molecules or fewer for most genes[41–43]. Since the limited number of reactant molecules can impact the rate of a chemical reaction in general, we sought the quantitative relationship of how mRNA numbers and co-translational protein targeting to mitochondria affect mitochondrial protein heterogeneity. To explore this, we analyzed the single molecule mRNA movement of *TIM50* mRNA with a relationship to mitochondria in live cells. We visualized mitochondria using mCherry linked to the mitochondrial matrix marker, Su9, while mRNAs were labeled with the MS2-MCP system. We reconstructed and analyzed the 3D mRNA movement trajectory using Mitograph V2.0 and Trackmate (ImageJ Plugin) in WT strains (Fig. 2A, Supplementary Fig. 2)[34]. We found that *TIM50* mRNAs localized to mitochondria (blue dots) showed restricted and slower movement as compared to freely moving mRNAs (red dots) (Fig. 2B). Moreover, the distance traveled by mRNA localized to the mitochondrial surface is also reduced compared to freely moving mRNAs (Fig. 2C, Supplementary Fig. 2). This leads mRNAs to remain localized to small mitochondrial regions for long periods. Collectively, these observations indicate that mitochondrial localization restricts the movement of *TIM50* mRNAs. Considering the half-life and abundance ratio of mRNA and protein, single mRNAs can produce tens to hundreds of proteins over an mRNA lifetime[44]. This suggests that the limited number of mRNA largely provides translated protein into a fixed number of mitochondria when the mitochondria become morphologically fragmented.

To explore the underlying causes of protein expression noise, we apply mathematical modeling (Fig. 2D). With a *TIM50* mRNA copy number of six[34] and a lifetime of 10 min[45,46], a mean of 54 mRNAs will be produced in a 90-minute generation, with a corresponding noise of 0.14 (Methods). If the number of proteins produced is proportional to mRNA produced, then protein numbers will have a similar noise due to mRNA production stochasticity of 0.14, similar to the minimum in Fig. 1G, setting a size-independent noise floor. Although bursty transcription would reduce the number of distinct mRNA production events necessary to produce an equal mRNA number and thus increase the noise contribution from mRNA production stochasticity, yeast
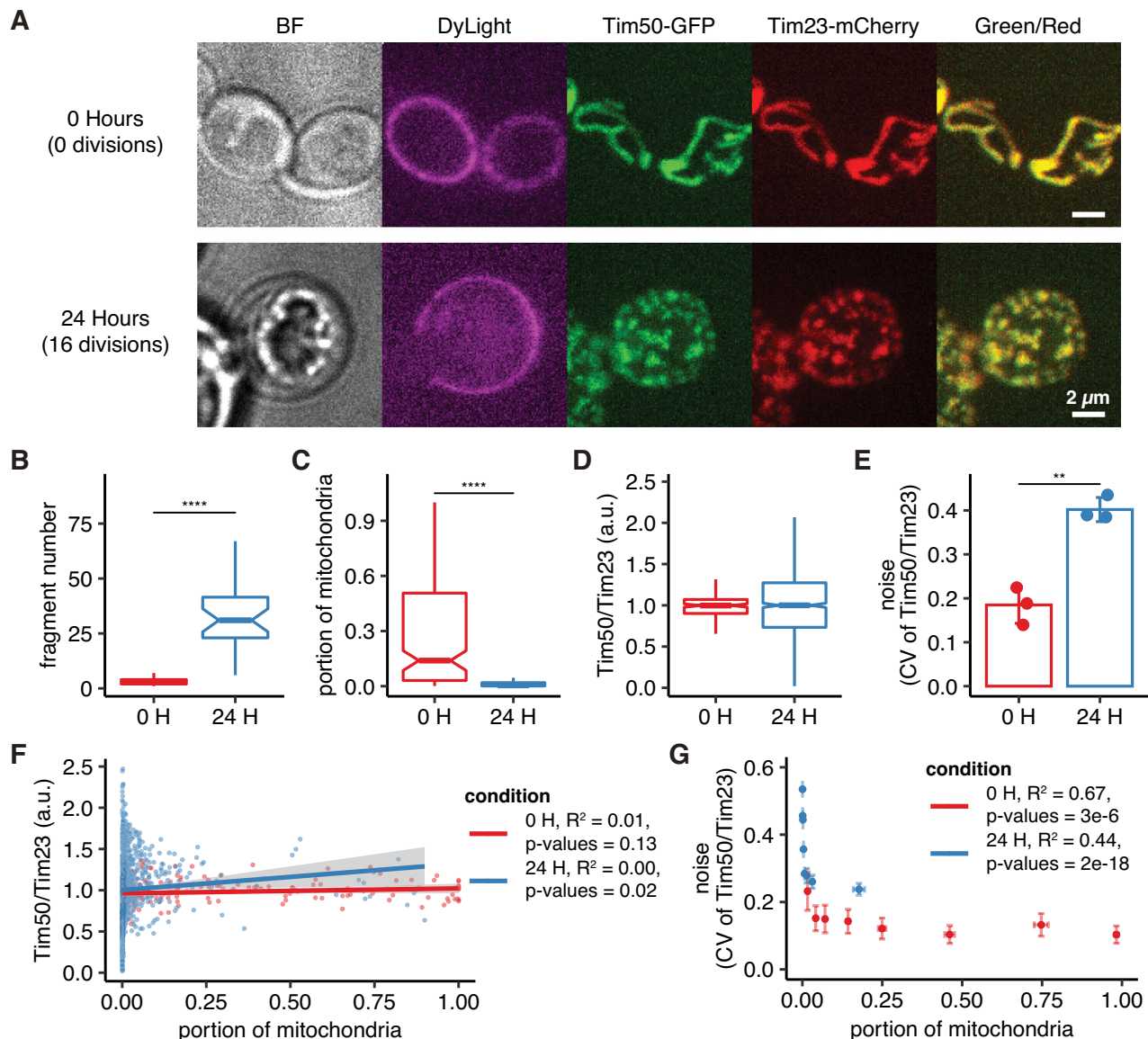
Fig. 1 | Aging increases the heterogeneity of mitochondrial protein distribution. A Protein distribution to each mitochondrial fragment in a young cell (top) and an aged cell (bottom). The cells of mother enrichment program strains marked with DyLight were analyzed at 0 h and 24 h after the addition of estradiol. The Tim50-GFP and Tim23-mCherry fluorescence was visualized by a spinning disc confocal microscope. BF: Bright field (center focal plane), DyLight, Tim50-GFP, Tim23-mCherry: z-projected images of each channel (Far-Red, GFP, RFP). Green/Red: merge of GFP and RFP channels. Scale bar, 2 μm. Images are the representation of three independent experiments. B The number of mitochondrial fragments per cell of the cells at 0 h and 24 h cells in A ($n > 30$, $P = 1.3E-14$). C The size of each mitochondrion was normalized as a portion of mitochondria per cell based on the sum of Tim23-mCherry intensity ($n > 30$, $P = 1.1E-61$). D The ratio distribution for the protein expression level of Tim50-GFP and Tim23-mCherry for each mitochondria fragment. The median was normalized to 1. (a.u. arbitrary units). Data presented as boxplots is denoted by the median, limits are the interquartile range

and whiskers correspond to 1.5 times the interquartile range (B–D). E The coefficient of variation (CV) or noise of data in D. The results represent the mean ± standard deviation of three independent experiments ($P = 0.002$). F The ratio distribution for the protein expression level of Tim50-GFP and Tim23-mCherry for each mitochondria fragment in D along with the portion of mitochondria. Each dot represents an individual mitochondrial fragment. The gray region surrounding the regression lines (two-sided) represent standard error of the mean (SEM). G The noise of F along with the portion of mitochondria. Each noise data point was calculated by dividing the population of individual mitochondrial fragments into eight groups. Error bars represent the SEM of three independent experiments. For F, G, R-squared values and p-values for the F statistic hypothesis test are shown on the side. The p-values were determined using the two-tailed Mann–Whitney test for B, C, Student's t test for E, and linear regression for F and G. Source data are provided as a Source Data file.

transcription appears to exhibit a small burst size[47,48], limiting such an increase. In contrast to noise associated with mRNA production, with protein delivery proportional to mitochondrial size, the noise associated with protein delivery will be inversely proportional to the square root of the mitochondrial portion size, such that this noise will decrease with increasing mitochondrial size with decreasing slope for larger mitochondrial fragments, similar to the trend observed in Fig. 1G. With post-translational protein delivery, there are a large

number of independent delivery events, leading the mitochondrial size-dependent noise from protein delivery to specific mitochondria to be relatively low. In contrast, with co-translational protein delivery, there are fewer protein delivery events, and the noise from protein delivery is relatively high. The stochasticity from mRNA production and protein delivery are combined in a stochastic simulation of two mitochondrial fragments (Fig. 2D). Post-translational protein delivery leads to noise independent of size and slightly above mRNA
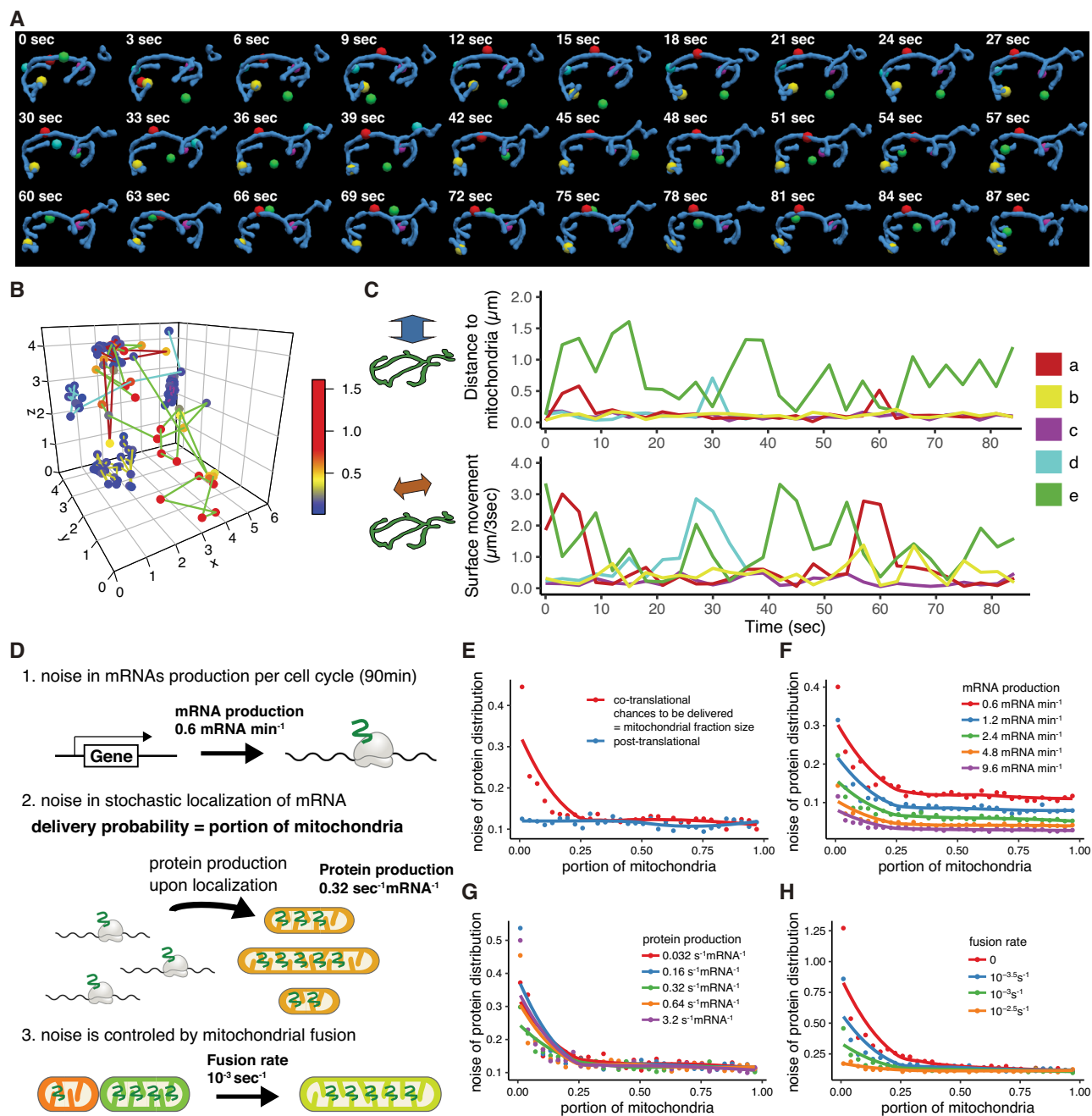
Fig. 2 | Stochastic nature of co-translational protein targeting increases the protein heterogeneity at the single mitochondrion. A Reconstruction of mitochondrial and *TimSO* mRNAs positional information in a single cell. Blue: mitochondria. The color particle and lines correspond to the same mRNAs (**A–C**). **B** The 3D trajectory of *TimSO* mRNA movements in a single cell. The colors of mRNA positions indicate the distance from the mitochondrial surface. Distance units for 3D trajectory and color bar indicating distance from mitochondria are in units of μm. **C** The 2D trajectory of *TimSO* mRNA movements regarding the distance to mitochondria (μm) and the horizontal movement to the mitochondrial surface (surface movement) in 3 s (μm/3 s). **D** A stochastic model description in which mitochondrial size and co-translational protein targeting with mitochondrial fission-fusion coordinate protein distribution using translational kinetic and molecular diffusion. Relationship between the noise of protein distribution and mitochondrial size of different protein import mechanisms (**E**), mRNA production rates (**F**), protein production rates (**G**), and fission-fusion rates (**H**) in the stochastic model. The trend line was calculated using a Loess regression. Source data are provided as a Source Data file.

production noise of 0.14 (Fig. 2E). In contrast, co-translational protein delivery leads to a size-dependent noise, with higher noise for small mitochondria (Fig. 2E) that can be increased by decreasing the mRNA production rate (Fig. 2F). It is interesting to note that the rate of protein production by each mRNA does not affect the noise (Fig. 2G). Mitochondrial fusion facilitates protein spread between mitochondria, such that with co-translational protein delivery, the mitochondrial size dependence of the noise is enhanced by a low mitochondrial fusion rate. Increasing the fusion rate compresses the size range over which noise increases to the smallest mitochondria, and at the highest mitochondrial fusion rates, the size dependence of noise is eliminated, with only noise due to mRNA production remaining (Fig. 2H). Stochastic simulations with dynamic mitochondrial networks of 30 fragments yield similar dependence on mitochondrial size and fusion rate (Supplementary Fig. 3A and Methods), as well as suggest that increased mitochondrial fragmentation due to decreased fusion in

older cells may lead to increased noise for smaller mitochondria, compared to equally small mitochondria in cells with less fragmented mitochondrial networks (Supplementary Fig. 3B, C and Methods). These findings suggest that the localization of mitochondrial mRNA and the co-translational delivery of proteins contribute to the noise in protein expression observed in small mitochondria and that this effect is amplified when the rate of mitochondrial fusion decreases.

Mitochondrial fusion dynamics maintain the homogeneous protein distribution

Mitochondrial morphological changes are dictated by the balance of fission-fusion reactions and mitophagy pathways maintained by

regulatory proteins[3,49]. To investigate whether mitochondrial fusion dynamics regulate the homogeneity of mitochondrial protein distribution, we used the fusion mutant, *fzo1Δ*. As expected, cells lacking Fzo1 exhibited fragmented mitochondrial morphology and a significant increase in the noise level of relative Tim50/Tim23 protein expression (Fig. 3A, B). Moreover, consistent with the above modeling (Fig. 2H), the noise level decreased substantially with an increase in the portion size of mitochondria in *fzo1Δ* cells (Fig. 3C). We next used the mitophagy deficient strain, *atg32Δ*, to examine the role of mitophagy in protein heterogeneity. In contrast to *fzo1Δ* cells, we found that *atg32Δ* cells showed no significant increase in mitochondrial fragmentation (Fig. 3D) or the noise level of relative Tim50/Tim23 protein
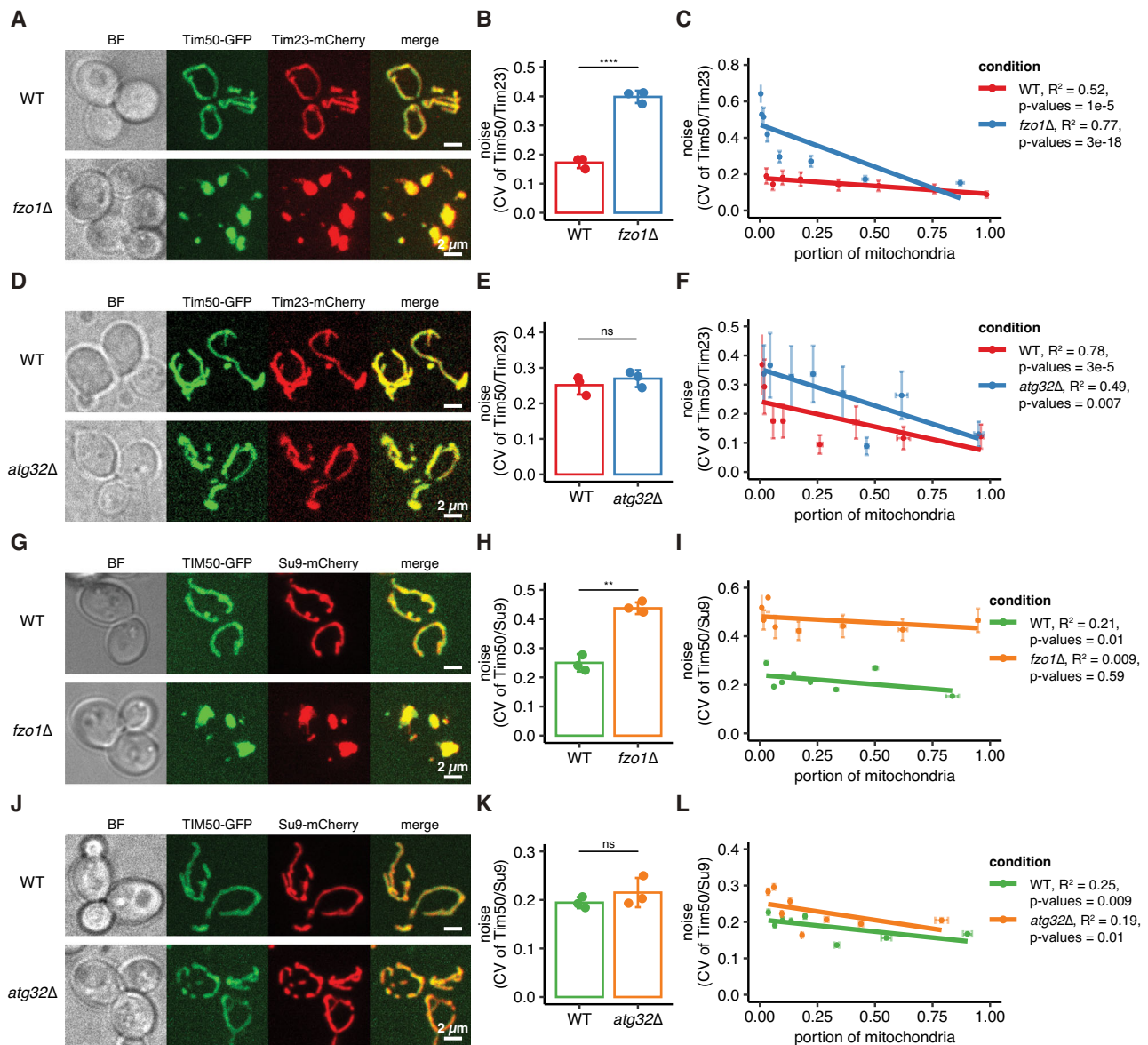

Fig. 3 | The heterogeneity of protein distribution is maintained by mitochondrial fission-fusion reaction and not through the mitophagy pathway. Protein distribution to each mitochondrial fragment in mutant strains: fission-mutant strain *fzo1Δ* (A–C, G–I), mitophagy-deficient strain *atg32Δ* (D–F, J–L) (n > 31). The fluorescence of Tim50-GFP and Tim23-mCherry (A–D) or Su9-mCherry (G–J) were visualized by a spinning disc confocal microscope. BF: Bright field (center focal plane), Tim50-GFP, Tim23-mCherry, Su9-mCherry: z-projected images of each channel (GFP, RFP). Merge: merge of GFP and RFP channels: scale bar, 2 μm.
B–E, H–K The noise of protein distribution in mutant strains. The results represent the mean ± standard deviation of three independent experiments. Statistical significance was evaluated by the two-tailed Student's *t* test ($P = 3.95E{-}05$ (B), $P = 0.003$ (H)). C– F, I– L Relationship between the noise of protein distribution and mitochondrial size in mutant strains. The noise value was calculated by dividing the population of individual mitochondrial fragments into eight groups. Error bars represent the SEM of three independent experiments. R squared values and *p*-values for the F statistic hypothesis test are shown on the side. Source data are provided as a Source Data file.

expression (Fig. 3E). Heterogeneity decreased with increasing mitochondrial portion size for *atg32Δ* cells, similar to the WT (Fig. 3F).

To further examine whether these regulatory relationships can be applied to general mitochondrial protein homeostasis, we tested two other mitochondrial proteins that are not components of an identical protein complex. We co-expressed Tim50-GFP and Su9-mCherry, a subunit 9 of mitochondrial ATPase of *Neurospora crassa*[50] conjugated with mCherry and localized to the mitochondrial matrix in yeast strains. We observed fragmented mitochondrial morphology and a significantly increased noise level in Tim50/Su9 relative protein expression in the *fzo1Δ* cells, compared to WT (Fig. 3G, H). Furthermore, Tim50/Su9 heterogeneity remains consistently high in fusion mutant cells, even for large mitochondrial portions (Fig. 3I). This is very different from the exponential relationship seen in the noise of Tim50/Tim23 (Fig. 3C). This suggests that when proteins do not form a complex, the homogeneity of proteins can easily be dysregulated. We observed a similar expression phenotype for relative Tim50/Su9 and Tim50/Tim23 proteins in *atg32Δ* cells (Fig. 3J-L). All the above evidence suggests that fission-fusion dynamics regulate heterogeneity in mitochondrial protein expression, and mitophagy may only have a minor influence on mitochondrial protein heterogeneity. These observations are not restricted to a specific protein complex as Tim50/Tim23 and Tim50/Su9 relative protein expression levels show similar noise level phenotypes as mitochondrial fusion dynamics change.

Inhibition of co-translational protein targeting prevents heterogeneous protein distribution

Next, we tested the two possible strategies to reduce heterogeneity in the protein distribution for smaller mitochondrial fragments. Our computational modeling showed that increasing the number of mRNA copies would reduce heterogeneity. To test this, we introduced a GFP-tagged *TIM50* integration plasmid with different copy numbers to control mRNA copy numbers. We observed that an increase in copy number decreased noise in the *fzo1Δ* cells, indicating reduced heterogeneity in mitochondrial protein composition (Fig. 4A). Doubling the mRNA copy number decreased noise by a factor of approximately 1.3 and tripling the copy number by approximately 1.8, similar to decreases predicted by modeling the mRNA production contribution to noise of 1.4 and 1.7, respectively. We further noticed that with an augmented expression of *TIM50* mRNA, there is a significant decrease in protein heterogeneity across all mitochondrial proportions (Fig. 4B), which was also seen in our simulations (Fig. 2F).

We then examined if altering co-translational delivery by directing localization of mitochondrially localized mRNA to other specific subcellular locations affects the heterogeneity of the protein distribution. We tested a tethering model where a CAAX-tagged MCP protein (MCP-CAAX) represented plasma membrane tethering (Fig. 4C)[34]. Since we previously observed that *fzo1Δ* strains lost the regulation of protein heterogeneity with an increase in mitochondrial proportion, we analyzed the effect of membrane tethering on protein heterogeneity in the *fzo1Δ* cells. We found that membrane tethering successfully rescued the phenotype, and protein heterogeneity was significantly decreased compared to the control strain (Fig. 4D, E).

To further strengthen the observation that increased heterogeneity results from protein import stochasticity and not from the redistribution of proteins in the mitochondria, we induced acute fragmentation using carbonyl cyanide 3-chlorophenylhydrazone (CCCP), which dissipates the mitochondrial membrane potential. No significant increase in protein heterogeneity was observed in the treatment groups compared to the control group (Fig. 4F, G), suggesting that acute fragmentation alone does not increase protein heterogeneity. Furthermore, this suggests that the measured changes in heterogeneity from sustained mitochondrial fragmentation are not an artifact of quantification errors from different size and shape distributions of mitochondria.

Finally, to explore if our model for the protein distribution noise applies to other co- and post-translationally targeted proteins, we analyzed the noise in several GFP-tagged yeast strains. As we have found that both mRNA expression and co-translational targeting can affect protein expression noise, we focused on proteins whose mRNA expression is similar to *Tim50* (Fig. 4H)[33,51,52]. These include the co-translationally localized proteins Mia40, Dld1, and Cox15, along with Pdx1 and Rsm7, which were post-translationally localized. We find that the two post-translationally targeted proteins exhibit significantly lower heterogeneity than all four of the co-translationally targeted proteins (Fig. 4I). Additionally, a consistent pattern emerged between noise and fragment size, with smaller fragments correlated with higher heterogeneity (Supplementary Fig. 4A). We further examined the components of the OXPHOS complex, including Atp7, Cox4, and Sdh4, whose mRNAs are post-translationally localized to the mitochondrial membrane and proteins are localized to cristae. These proteins formed distinct puncta on the mitochondrial membrane and demonstrated consistently high noise, independent of their expression levels (Supplementary Fig. 4B–D and 5J).

Collectively, the results indicate that co-translational protein localization consistently correlates with increased mitochondrial protein heterogeneity, which can be inhibited by increasing the transcriptional level or limiting the co-translational protein delivery.

Discussion

Aging is associated with increased mitochondrial fragmentation and a decline in mitochondrial function across many species. Here, we report that the physical changes associated with mitochondrial fragmentation lead to heterogeneity in protein distribution due to mRNA localization and co-translational protein delivery (Fig. 5A, B). Our two-color fluorescent reporter gene analysis based on quantitative microscopy shows that mitochondrial proteins, even components of the same complex, are heterogeneously distributed to each mitochondrion in aged cells (Fig. 1). There is an increase in heterogeneity as mitochondrial fragments become smaller. We observed that single-molecule *TIM50* mRNAs, which encode a co-translationally imported protein, remain stably associated with mitochondria, which suggests co-translational protein import may restrict protein production to specific mitochondrial fragments (Fig. 2A–C). Using computational modeling, we found that the generation of heterogeneity can largely be explained by the stochastic nature of compartmentalization, and co-translational protein delivery is the main contributor to the high heterogeneity (Figs. 2D-H and 5C). The heterogeneity of protein distribution was increased in mitochondrial fusion deficient *fzo1Δ* but not in the mitophagy deficient *atg32Δ* (Fig. 3). This indicates that cells repress heterogeneity of protein distribution mainly by maintaining mitochondrial fission-fusion reactions and not through the mitophagy pathway. Lastly, we showed ways to reduce the noise level by either increasing the transcriptional level or limiting co-translational protein delivery (Fig. 4A–E, I).

We generally see highly complex mitochondrial networks maintained with mitochondrial fission and fusion dynamics across various cell types and conditions[3,12]. We showed that a large and dynamic mitochondrial network structure, effectively forming a connected compartment, reduces noise levels by mixing the components across the mitochondrial network (Figs. 1G, 3C, F, I, L and 4B–E). In particular, we found that mitochondrial fission and fusion reactions are essential to reduce mitochondrial protein distribution noise generated by mitochondrial fragmentation and co-translational protein delivery (Fig. 3B–H). Our results suggest that when proteins do not form a complex, the heterogeneity in a single mitochondrial fragment can be substantially higher than when the proteins are part of the same complex (Fig. 3C–I). This suggests that there may be pathways that inhibit protein heterogeneity of proteins forming complexes, such as protein degradation of excess subunits[53]. While this study did not show

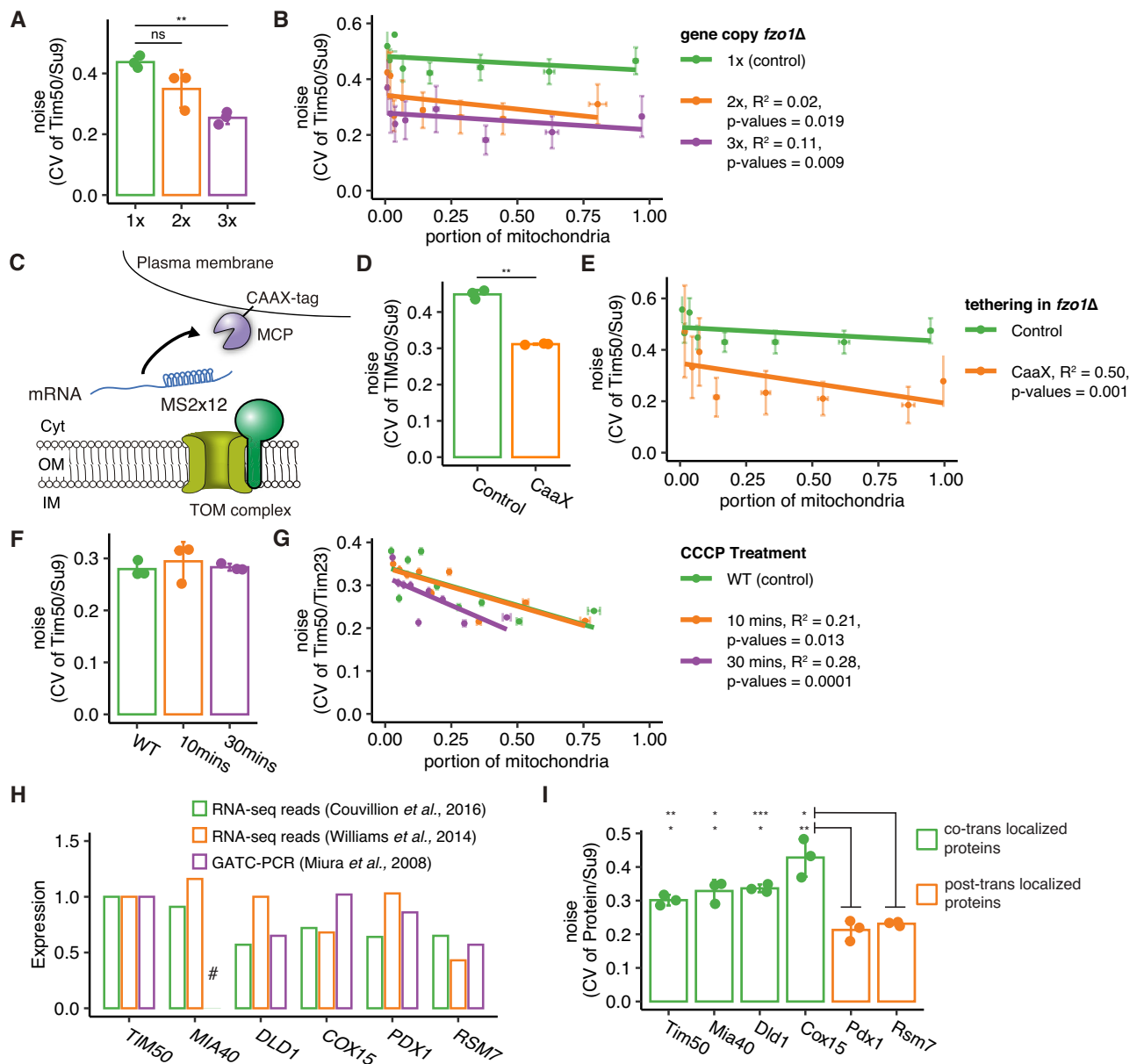**Fig. 4 | Co-translational protein delivery regulates protein composition. A** The noise of protein distribution with variable copy numbers (1x, 2x, 3x) of GFP-tagged Tim50 integration plasmid in *fzo1Δ* strain (n > 46). The results represent the mean ± standard deviation of three independent experiments (P = 0.006 (1x − 3x)). **B–E, G** Relationship between the noise of protein distribution and mitochondrial size in **A–D**, and **F**. The noise value was calculated by dividing the population of individual mitochondrial fragments into eight groups. Error bars represent the SEM of three independent experiments. R squared values and *p*-values for the F statistic hypothesis test are shown on the side. **C** Schematic representation of plasma membrane tethering models. In plasma membrane tethering, MCP is bound to CAAX (a ras protein family member). **D** The noise of protein distribution in plasma membrane tethering (CAAX) of GFP-tagged Tim50 integration plasmid in *fzo1Δ* strain (n > 47). The results represent the mean ± standard deviation of three independent experiments (P = 0.002). **F** The noise of protein distribution of GFP-tagged Tim50 upon CCCP treatment in WT (No drug), 10 min, and 30 min (n > 64). The results represent the mean ± standard deviation of three independent experiments. **H** RNA expression from previously published studies normalized to *TIM50* mRNA expression (# not available). **I** The noise of protein distribution of GFP-tagged proteins. Green bar represents co-translationally localized mitochondrial proteins. Orange bar represents post-translationally localized mitochondrial proteins (n > 40). Each co-translationally localized protein was compared to both post-translationally localized controls (Pdx1 and Rsm7) (Tim50 (P = 0.02 and 0.009), Mia40 (P = 0.01 and 0.03), Dld1 (P = 0.01 and 0.0007), Cox15 (P = 0.009 and 0.02). Statistical significance was assessed using the two-tailed Student's *t* test for **D** and two-tailed Anova followed by t-test for pairwise comparison for **A–F** and **I**. Source data are provided as a Source Data file.

a significant influence of the mitophagy pathway, the heterogeneity of the protein distribution throughout mitochondria (Fig. 3E–K), regulation of protein production, and protein degradation may also contribute to more exact stoichiometries[54,55].

Early observations of inducible fragmentation due to loss of Fzo1 function revealed that long-term fragmentation leads to loss of mtDNA and membrane potential; however, these phenotypes are not apparent

immediately after fragmentation[56]. This suggests that structural fragmentation alone does not drive mitochondrial dysfunction but is caused by processes that occur over extended periods. As reported here, the nuclear-encoded mRNA noise-driven heterogeneity is a distinct proposal from stochasticity in mtDNA or mitophagy controlling heterogeneity and downstream dysfunction. Our observation indicates that co-translational protein targeting plays a significant role in
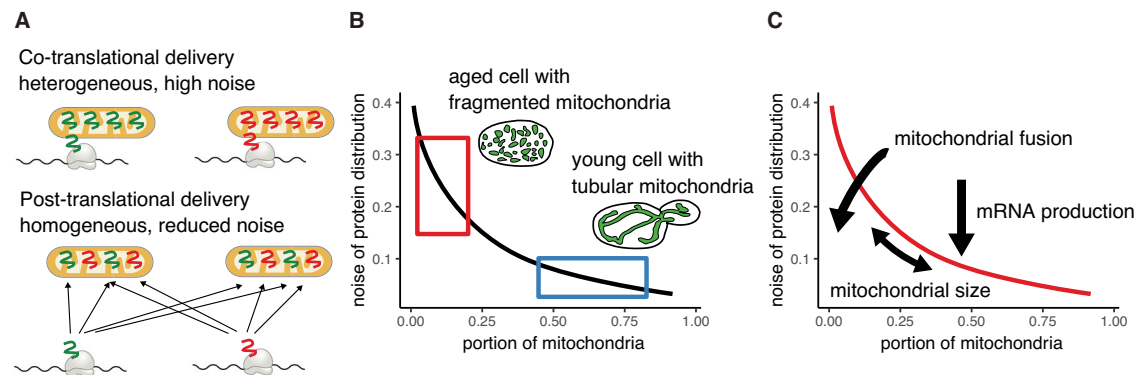
Fig. 5 | Mitochondrial fragmentation causes heterogeneity in protein distribution via mRNA localization and co-translational protein delivery. A A schematic model description of different protein delivery mechanisms. Co-translational protein delivery increases protein distribution heterogeneity, while post-translational delivery reduces the noise in protein distribution. **B** Aged cells with fragmented mitochondria show higher noise, while young cells with tubular network mitochondrial structure show lower noise. **C** A schematic model description of mitochondrial protein distribution. Upon co-translational protein delivery, mitochondrial size influences stochastic mRNA localization. An increase in mitochondrial fission-fusion rates or mRNA production rates will each independently reduce protein distribution noise.

generating protein heterogeneity. Even a slight initiation of mitochondrial fragmentation can have noticeable consequences due to the limited number of mRNA copy numbers compared to mtDNAs. From ~25% to over 50% of nuclear-encoded mitochondrial mRNAs are localized to the mitochondria across both fermentative and respiratory conditions[28,33,57]. With >100 mRNAs being localized even in fermentative conditions, the associated heterogeneity in protein expression due to co-translational insertion could be a strong driver of mitochondrial dysfunction as individual mitochondria deviate from the optimal stoichiometry of mitochondrial protein complexes. These postulate that overall mitochondrial dysfunction is introduced not only by mtDNA and mitophagy but also by co-translational protein targeting, which accelerates the dysfunction. Research is underway to better describe how mitochondrial fragmentation and co-translational protein import impact mitochondrial proteostasis. Elucidating the genetic regulatory mechanisms governing co-translational protein import and identifying potential inhibitors of this process are essential for advancing this research frontier. As many human diseases and aging are associated with mitochondrial dysfunction, it is also necessary to determine whether there is a similar association between the degree of mitochondrial fragmentation and mitochondrial protein heterogeneity in human cells. Further studies focusing on this molecular mechanism could contribute to treating mitochondria-related diseases.

Methods
Yeast strains and plasmids
The yeast strains and plasmids used are listed in Supplementary Table 1, and the oligonucleotides used for plasmid construction and gene modification are listed in Supplementary Table 2. To reduce variability among the constructed yeast strains, the strains were created either through the integration of a linear PCR product or a plasmid linearized through restriction digest. Tim50-GFP was expressed by *TIM50* promoter from integrated plasmid TTP155. The copy number of integrated plasmids in a cell were tested through microscopy screening, and the strains with one copy of integration were used for all the experiments except Fig. 4. Fluorescent protein tagging for *TIM23* was performed with PCR-mediated homologous recombination using pFA6a-link-yomCherry-SpHis5[58] and integrations were confirmed by PCR.

Su9-mCherry was expressed by TDH3 promoter from integrated plasmid TTP076, and the strains with three copies of integrated plasmids in a cell were screened through microscopy and used for further experiments. Fluorescent protein tagging for other proteins used in the study including Mia40, Dld1, Cox15, pdx1, Rsm7, Atp7, Cox4, and Sdh4 was performed with PCR-mediated homologous recombination

using pFA6a-link-yoEGFP-CaURA3, and integrations were confirmed by microscopy[58]. Deletion mutant strains were constructed with PCR-mediated homologous recombination using pFA6a-hphMX6[59], and integrations were confirmed by PCR. Plasma membrane anchor MCP-iRFP-CaaX (TTP223) was constructed by swapping the GFP of TTP167 with the iRFP of TTP145 through the combination of Gibson assembly and PCR[34]. The strains expressing MCP-iRFP-CaaX from two sets of integrated plasmids were selected through microscopy screening and used for further experiments.

Microscopy
Image data for C-terminal integrated fluorescent proteins were collected as follows: Yeast cells were grown in the YPAD (YPA medium containing 2% glucose) with a 15 ml glass tube at 30 °C with rotator speeds of 60 rpm. 100 μl of mid-log phase wild-type yeast cells (OD600 of 0.4–0.7) were harvested and placed into a 96-well Glass Bottom Plate (Cellvis LLC) coated with 0.1 mg/mL concanavalin A (Sigma-Aldrich C2010). For the aging experiment, we used mother enrichment program (MEP) strains, which were controlled by the addition of estradiol (final 1 μM) (Sigma-Aldrich E2758). Cells were imaged at 23 °C with 3-second intervals by an Eclipse Ti2-E Spinning Disk Confocal with Yokogawa CSU-X1 (Yokogawa) with 50 μm pinholes, located at the Nikon Imaging Center UCSD. Imaging was performed using SR HP APO TIRF 100 × 1.49 NA oil objective with the correction collar set manually for each experiment (pixel size 0.0936 μm). Z-stacks (200 nm steps) were acquired by a Prime 95B sCMOS camera (Photometrics). Imaging was controlled using NIS-Elements software (Nikon). Image data for Fig. 3D–F, 4F, G, and 4I were imaged at 23 °C by an Eclipse Ti2-E Spinning Disk Confocal with Yokogawa CSU-W1 (Yokogawa) with 50 μm pinholes, located at the Tsinghua-SIGS Tsuboi Laboratory. Imaging was performed using CFI Plan Apochromat Lambda 100 × 1.49 NA oil objective. Z-stacks (200 nm steps) were acquired by a Prime 95B sCMOS camera (Photometrics) (pixel size 0.11 μm). Imaging was controlled using NIS-Elements software (Nikon). Single-molecule mRNA visualization with mitochondria was performed as follows: Yeast cells were grown in the YPAD with a 15 ml glass tube at 30 °C with rotator speeds of 60 rpm. 300 μl of mid-log phase wild-type yeast cells (OD600 of 0.4–0.7), grown in an appropriate medium, were harvested and placed into a Y04C microfluidic chamber controlled by the CellASIC Onix system. 300 μl YPAD were put into the flow-wells, the chambers were loaded with cells at 3 psi, and the medium continuously flowed at 3 psi. Cells were imaged at 30 °C with a Yokogawa CSU-X1 Spinning Disk Confocal (Solamere Technology Group) mounted on a Nikon Eclipse Ti chassis

motorized inverted microscope located at the Department of Developmental & Cell Biology UCI. Imaging was performed using a 100x/1.49 NA oil APO TIRF objective with the correction collar set manually for each experiment and a 1x tube lens (pixel size 0.084 μm). Z-stacks (300 nm steps) were acquired in the fluorescent channel (33 ms exposure) on a Hamamatsu electron-multiplying charge-coupled device (EMCCD) camera. Imaging was controlled using MicroManager ImageAcquisition (v1.4.16). The experiments for Figs. 3G–I, 4A, B, and 4D, E were conducted on the same day.

Quantification of protein expression in each mitochondrion from image data

The expression level of GFP-tagged mitochondrially localized proteins was quantified using a custom analysis pipeline, as depicted in Supplementary Fig. 1. The MitoGraph 3.1 software was applied to the mCherry channel to segment the mitochondria morphology, and the resulting 3D binary mask was then used to segment the GFP and mCherry channels of individual mitochondria (available at https://github.com/vianamp/MitoGraph). "*Find Connected Regions*" (ImageJ Plugin) was used to identify each individual mitochondrial fragment in the network. The sum of the intensity of the GFP and mCherry channel covered by a 3D binary mask from each mitochondrion was measured using a custom ImageJ script. The scripts, along with their requirements and usage instructions, can be accessed at https://github.com/khan-ah. The protein expression levels in different conditions are summarized in Supplementary Fig. 5.

The increased Tim50/Tim23 signal heterogeneity in fragmented mitochondria can result from different size and shape distributions of mitochondria in fused vs fragmented phenotypes. To address this, we generated a dataset by selecting the larger mitochondrial fragments (portion of mitochondria ≥0.50) and measuring the intensities of portions on each slice individually i.e., smaller portions of mitochondria. The noise observed in those smaller ROIs was not significantly different than that of larger fragments in neither old compared to young (Supplementary Fig. 6A) nor *fzo1Δ* compared to WT strains (Supplementary Fig. 6C). Consistently, mean noise also showed no significant difference (Supplementary Fig. 6B–D). The results suggest that the increased noise in age-associated fragmentation is not the consequence of measurement stochasticity. Raw data for these experiments can be found in Supplementary Data 1.

Reconstruction of 3D mitochondria and mRNA visualization

To allow accurate visualization of mRNA molecules, multiple MS2 stem-loops are inserted in the 3'-UTR of the mRNA of interest and are recognized by the MCP-GFP fusion protein[60,61]. We improved this system by titrating the MCP-GFP levels until we observed single-molecule mRNA foci[34]. We then performed rapid 3D live cell imaging using spinning disk confocal microscopy. We reconstructed and analyzed the spatial relationship between the mRNAs and mitochondria using the custom ImageJ plugin Trackmate[62] and MitoGraph V2.0[34,63,64]. We measured the distance between mRNA and mitochondria by finding the closest meshed surface area of the mitochondria matrix[34]. The code used for the analysis is available from https://github.com/tsuboitat.

mRNA production and protein delivery noise modeling

If mRNA is produced at a constant rate, the number of mRNA produced over a generation time period will be Poisson-distributed. With a *TIM50* mRNA copy number of approximately six[34] and a lifetime of approximately 10 min[46], 54 mRNAs will be produced on average in a 90-min generation. Poisson-distributed processes have an equal mean and variance, such that the coefficient of variation is the inverse square root of the mean of 54 or a coefficient of variation of 0.14 for isolated mRNA production noise.

Bursty transcription could lead to the same number of mRNA being produced over fewer distinct mRNA production events, leading to greater stochasticity in mRNA and downstream protein production. Experiments suggest that few yeast genes exhibit bursty transcription[47]. Experiments show that *GAL10* yeast genes have a mean burst size of two transcripts[48]. Although we are not aware of *TIM50* transcription burst size measurements, if *TIM50* similarly had a burst size of two transcripts, then we would expect the coefficient of variation to increase to approximately 0.19.

For isolated protein delivery noise, we consider proteins delivered to mitochondria in N_{del} delivery events, with each mitochondrion selected with a probability proportional to the mitochondrial size. With the mitochondrial size that is a fraction f of the total mitochondrial size in the cell, then for Poisson-distributed delivery events, a mitochondrion will have a mean and variance of fN_{del} delivery events, and thus a fractional size f-dependent coefficient of variation of $(fN_{del})^{-1/2}$. If each mRNA docks at one mitochondrion and delivers all its translated proteins to that mitochondrion, then the size-dependent coefficient of variation over a generation is $(fN_{del})^{-1/2} = (54\,f)^{-1/2}$. For mRNA that does not dock at a mitochondrion, each translated protein stochastically selects a mitochondrion proportional to its size, with the copy number of 4000 Tim50 proteins[27], each generation the coefficient of variation is $(fN_{del})^{-1/2} = (4000\,f)^{-1/2}$.

In silico experiment (stochastic simulation)

mRNA production and decay, protein production and decay, mitochondrial fusion, and cell division are all stochastically simulated for two mitochondria, one of fractional size f and the other with fractional size 1−f, with the Gillespie algorithm[65,66]. Two mitochondria are the mean number of connected components in yeast mitochondrial networks[67]. With *TIM50* mRNA copy number of approximately 5[34] and mRNA lifetime of approximately 10 min[46], then mRNA is produced at the rate of 5/lifetime, and each mRNA decays at the rate of 1/lifetime. Proteins are produced at a rate of 0.13/s per *TIM50* mRNA, corresponding to the rate at which 4000 proteins will typically be present immediately prior to division and similar to an earlier estimate of the rate of *TIM50* translation initiation of 0.126/s[68]. Each protein decays at a rate of 1/7200 per second, corresponding to a 2-h lifetime[69]. For the model of co-translational protein delivery to mitochondria, mRNA selects a mitochondrion when produced and delivers all proteins to that mitochondrion. For post-translational protein delivery to mitochondria, a mitochondrion for the protein to be delivered is selected for each protein produced. Mitochondrial fusion is represented in the model by events that equalize mitochondrial protein concentrations across mitochondria, occurring at a certain rate. We explore fusion event rates of zero and the range of $10^{-3.5}$–$10^{-2.5}$/s, similar to experimentally estimated mitochondrial fusion rates[25,70,71]. Cell division is implemented by instantly halving the protein numbers in each mitochondrion every generation period of 90 min. Data shown in Fig. 2E–G is after simulating for ten generations.

We also simulated mRNA production and decay, protein production and decay, mitochondrial fusion, and cell division on dynamic mitochondrial networks by modifying the quantitative model described by Sukhorukov et al.[70], for 30 mitochondrial fragments. Fused mitochondrial fragments share proteins to equalize their protein concentration. For the medium fusion case of Supplementary Fig. 3A, we used a fission rate of $10^{-3}\,s^{-1}$ for each end-to-end fused connection of two mitochondrial fragments and a fission rate of $1.5 \times 10^{-3}\,s^{-1}$ for each end-to-side connection of three mitochondrial fragments, aligning with the two-fragment model and experimental fusion rates. The end-to-end and end-to-side fusion rates of the model were then chosen to be $10^{-5}\,s^{-1}$ and $5 \times 10^{-4}\,s^{-1}$ per available fragment pair to provide a range of connected mitochondrial sizes. The 30-fragment model data for protein concentration noise vs portion of mitochondria is very similar to the two-fragment model for variation in fusion and fission rates. As the low and high fusion rate data in Supplementary Fig. 3A has all fission and fusion rates multiplied by $10^{-0.5}$ and $10^{0.5}$, respectively,

the network connectivity is unchanged between low, medium, and high fusion rates. In Supplementary Fig. 3B, we varied the balance between fusion and fission rates by changing fusion rates, which alters the mitochondrial network connectivity, finding that less-connected networks yielded higher protein concentration noise, particularly for smaller mitochondria – this result aligns with the higher noise seen in older cells with more fragmented mitochondrial networks and in cells with mitochondrial fusion defects. Supplementary Fig. 3B used the parameters of medium fission-fusion rate from Supplementary Fig. 3A for medium fragmentation, with low fragmentation increasing both end-to-end and end-to-side fusion rates by a factor 2 and high and higher fragmentation decreasing fusion rates by factors of 2 and 4, respectively. In Supplementary Fig. 3C, we varied the mitochondrial network connectivity by changing fission rates, finding that more- or less-connected mitochondrial networks had quite similar protein concentration noise, even for smaller mitochondria, which does not align with the higher noise seen in older cells or cells with mitochondrial fusion defects. Supplementary Fig. 3C used the parameters of medium fission-fusion rate from Supplementary Fig. 3A for medium fragmentation, with low fragmentation decreasing end-to-end and end-to-side fission rates by a factor 2 and high and higher fragmentation increasing fission rates by factors of 2 and 4, respectively. These results suggest that the mitochondrial networks of older cells become fragmented through less fusion rather than more fission.

Statistics and reproducibility

Graphs and statistical analyses were performed using R (4.3.3). No statistical method was used to predetermine sample size. Outliers in datasets were assessed and excluded using Grubbs' test. Values are expressed as means ± SD for three independent experiments data and as means ± SEM for all the other scenarios. Differences between values were examined using the two-tailed Mann–Whitney test, Student's t test, and Anova followed by t-test for pairwise comparison and are specified in the figure legends. Values were considered significant at $P < 0.05$.

Reporting summary

Further information on research design is available in the Nature Portfolio Reporting Summary linked to this article.

Data availability

All data supporting the findings of this study are available within the paper and its supplementary information. All the raw and generated in this study are provided in the Supplementary Information/Source Data file (Supplementary Data 1). Further information and requests for resources, scripts, and reagents should be directed to and will be fulfilled by the lead contact, T.T. (ttsuboi@sz.tsinghua.edu.cn). Source data are provided with this paper.

Code availability

The code for analyzing the intensity of mitochondrial fragments is available at https://github.com/khan-ah. The code for the stochastic modeling of protein distribution noise and mitochondrial size under different protein import mechanisms, mRNA production rates, protein production rates, and fission-fusion rate is available at https://github.com/aidanbrowntmu/mitoheterogeneity. The code for MitoGraph is available at https://github.com/vianamp/MitoGraph. The code for measuring the distance between single particles in 3D is available at https://github.com/tsuboitat.

References

1. Spinelli, J. B. & Haigis, M. C. The multifaceted contributions of mitochondria to cellular metabolism. *Nat. Cell Biol.* **20**, 745–754 (2018).
2. Eisner, V., Picard, M. & Hajnóczky, G. Mitochondrial dynamics in adaptive and maladaptive cellular stress responses. *Nat. Cell Biol.* **20**, 755–765 (2018).
3. Westermann, B. Mitochondrial Fusion and Fission in Cell Life and Death. *Nat. Rev. Mol. Cell Biol.* **11**, 872–884 (2010).
4. das Neves, R. P. et al. Connecting variability in global transcription rate to mitochondrial variability. *PLoS Biol.* **8**, e1000560 (2010).
5. Johnston, I. G. et al. Mitochondrial variability as a source of extrinsic cellular noise. *PLoS Comput. Biol.* **8**, 35–37 (2012).
6. El-Hattab, A. W. & Scaglia, F. Mitochondrial DNA Depletion Syndromes: Review and Updates of Genetic Basis, Manifestations, and Therapeutic Options. *Neurotherapeutics* **10**, 186–198 (2013).
7. Aryaman, J., Johnston, I. G. & Jones, N. S. Mitochondrial heterogeneity. *Front. Genet.* **10**, 1–16 (2019).
8. Chen, H. et al. Mitochondrial fusion is required for mtdna stability in skeletal muscle and tolerance of mtDNA mutations. *Cell* **141**, 280–9 (2010).
9. Johnston, I. G. & Jones, N. S. Closed-form stochastic solutions for non-equilibrium dynamics and inheritance of cellular components over many cell divisions. *Proc. R. Soc. A Math. Phys. Eng. Sci.* **471**, 280–289 (2015).
10. Stephan, T. et al. MICOS assembly controls mitochondrial inner membrane remodeling and crista junction redistribution to mediate cristae formation. *EMBO J.* **39**, 1–24 (2020).
11. Jimenez, L., Laporte, D., Duvezin-Caubet, S., Courtout, F. & Sagot, I. Mitochondrial ATP synthases cluster as discrete domains that reorganize with the cellular demand for oxidative phosphorylation. *J. Cell Sci.* **127**, 719–726 (2014).
12. Jakubke, C. et al. Cristae-dependent quality control of the mitochondrial genome. *Sci. Adv.* **7**, eabi8886 (2021).
13. Gerencser, A. A. et al. Quantitative measurement of mitochondrial membrane potential in cultured cells: calcium-induced de- and hyperpolarization of neuronal mitochondria. *J. Physiol.* **590**, 2845–2871 (2012).
14. Gerencser, A. A., Mookerjee, S. A., Jastroch, M. & Brand, M. D. Measurement of the Absolute Magnitude and Time Courses of Mitochondrial Membrane Potential in Primary and Clonal Pancreatic Beta-Cells. *PLoS One* **11**, e0159199 (2016).
15. Wang, W. et al. Superoxide Flashes in Single Mitochondria. *Cell* **134**, 279–290 (2008).
16. Santo-Domingo, J., Giacomello, M., Poburko, D., Scorrano, L. & Demaurex, N. OPA1 promotes pH flashes that spread between contiguous mitochondria without matrix protein exchange. *EMBO J.* **32**, 1927–1940 (2013).
17. Yoon, Y., Galloway, C. A., Jhun, B. S. & Yu, T. Mitochondrial dynamics in diabetes. *Antioxid. Redox Signal* **14**, 439–457 (2011).
18. Galloway, C. A. & Yoon, Y. Mitochondrial morphology in metabolic diseases. *Antioxid. Redox Signal* **19**, 415–430 (2013).
19. Gao, J. et al. Abnormalities of Mitochondrial Dynamics in Neurodegenerative Diseases. https://doi.org/10.3390/antiox6020025 (2017).
20. Liu, Y. J., McIntyre, R. L., Janssens, G. E. & Houtkooper, R. H. Mitochondrial fission and fusion: A dynamic role in aging and potential target for age-related disease. *Mech. Ageing Dev.* **186**, 111212 (2020).
21. Zhao, J. et al. Mitochondrial dynamics regulates migration and invasion of breast cancer cells. *Oncogene* **32**, 4814–4824 (2013).
22. Xu, K. et al. MFN2 suppresses cancer progression through inhibition of mTORC2/Akt signaling. *Sci. Rep.* **7**, 41718 (2017).
23. Li, Y. et al. A programmable fate decision landscape underlies single-cell aging in yeast. *Science* https://doi.org/10.1126/science.aax9552 (2020).
24. Hughes, A. L. & Gottschling, D. E. An early age increase in vacuolar pH limits mitochondrial function and lifespan in yeast. *Nature* **492**, 261–265 (2012).

25. Twig, G. et al. Fission and selective fusion govern mitochondrial segregation and elimination by autophagy. *EMBO J.* **27**, 433–446 (2008).

26. Hoitzing, H., Johnston, I. G. & Jones, N. S. What is the function of mitochondrial networks? A theoretical assessment of hypotheses and proposal for future research. *BioEssays* **37**, 687–700 (2015).

27. Morgenstern, M. et al. Definition of a High-Confidence Mitochondrial Proteome at Quantitative Scale. *Cell Rep.* **19**, 2836–2852 (2017).

28. Marc, P. et al. Genome-wide analysis of mRNAs targeted to yeast mitochondria. *EMBO Rep.* **3**, 159–164 (2002).

29. Saint-Georges, Y. et al. Yeast mitochondrial biogenesis: a role for the PUF RNA-binding protein Puf3p in mRNA localization. *PLoS One* **3**, e2293 (2008).

30. Gadir, N., Haim-Vilmovsky, L., Kraut-Cohen, J. & Gerst, J. E. Localization of mRNAs coding for mitochondrial proteins in the yeast Saccharomyces cerevisiae. *RNA* **17**, 1551–1565 (2011).

31. Garcia, M. et al. Mitochondria-associated yeast mRNAs and the biogenesis of molecular complexes. *Mol. Biol. Cell* **18**, 362–368 (2007).

32. Fazal, F. M. et al. Atlas of Subcellular RNA Localization Revealed by APEX-Seq. *Cell* **178**, 473–490.e26 (2019).

33. Williams, C. C., Jan, C. H. & Weissman, J. S. Targeting and plasticity of mitochondrial proteins revealed by proximity-specific ribosome profiling. *Science* **346**, 748–751 (2014).

34. Tsuboi, T. et al. Mitochondrial volume fraction and translation speed impact mRNA localization and production of nuclear-encoded mitochondrial proteins. *Elife* **9**, 1–24 (2020).

35. Eliyahu, E. et al. Tom20 Mediates Localization of mRNAs to Mitochondria in a Translation-Dependent Manner. *Mol. Cell Biol.* **30**, 284–294 (2010).

36. Lesnik, C., Cohen, Y., Atir-Lande, A., Schuldiner, M. & Arava, Y. OM14 is a mitochondrial receptor for cytosolic ribosomes that supports co-translational import into mitochondria. *Nat. Commun.* **5**, 1–10 (2014).

37. Borst, P. & Grivell, L. A. The Mitochondrial Genome of Yeast. *Cell* **15**, 705–723 (1978).

38. Palmer, C. S., Anderson, A. J. & Stojanovski, D. Mitochondrial protein import dysfunction: mitochondrial disease, neurodegenerative disease and cancer. *FEBS Lett.* 595, https://doi.org/10.1002/1873-3468.14022 (2021).

39. Demishtein-Zohary, K. & Azem, A. The TIM23 mitochondrial protein import complex: function and dysfunction. *Cell Tissue Res.* 367, https://doi.org/10.1007/s00441-016-2486-7 (2017).

40. Lindstrom, D. L. & Gottschling, D. E. The mother enrichment program: A genetic system for facile replicative life span analysis in Saccharomyces cerevisiae. *Genetics* **183**, 413–422 (2009).

41. Brennan, C. M. et al. Protein aggregation mediates stoichiometry of protein complexes in aneuploid cells. *Genes Dev.* **33**, 1031–1047 (2019).

42. Miura, F. et al. Absolute quantification of the budding yeast transcriptome by means of competitive PCR between genomic and complementary DNAs. *BMC Genomics* **9**, 1–14 (2008).

43. Lahtvee, P. J. et al. Absolute Quantification of Protein and mRNA Abundances Demonstrate Variability in Gene-Specific Translation Efficiency in Yeast. *Cell Syst.* **4**, 495–504.e5 (2017).

44. Marguerat, S. et al. Quantitative analysis of fission yeast transcriptomes and proteomes in proliferating and quiescent cells. *Cell* **151**, 671–683 (2012).

45. Munchel, S. E., Shultzaberger, R. K., Takizawa, N. & Weis, K. Dynamic profiling of mRNA turnover reveals gene-specific and system-wide regulation of mRNA decay. *Mol. Biol. Cell* **22**, 2787–2795 (2011).

46. Chan, L. Y., Mugler, C. F., Heinrich, S., Vallotton, P. & Weis, K. Non-invasive measurement of mRNA decay reveals translation initiation as the major determinant of mRNA stability. *Elife* **7**, 1–32 (2018).

47. Zenklusen, D., Larson, D. R. & Singer, R. H. Single-RNA counting reveals alternative modes of gene expression in yeast. *Nat. Struct. Mol. Biol.* **15**, 1263–1271 (2008).

48. Lenstra, T. L., Coulon, A., Chow, C. C. & Larson, D. R. Single-Molecule Imaging Reveals a Switch between Spurious and Functional ncRNA Transcription. *Mol. Cell* **60**, 597–610 (2015).

49. Onishi, M., Yamano, K., Sato, M., Matsuda, N. & Okamoto, K. Molecular mechanisms and physiological functions of mitophagy. *EMBO J.* **40**, e104705 (2021).

50. Schmidt, B., Hennig, B., Zimmermann, R. & Neupert, W. Biosynthetic pathway of mitochondrial ATPase subunit 9 in Neurospora crassa. *J. Cell Biol.* **96**, 248–255 (1983).

51. Couvillion, M. T., Soto, I. C., Shipkovenska, G. & Churchman, L. S. Synchronized translation programs across compartments during mitochondrial biogenesis. *Nature* **533**, 499 (2016).

52. Miura, F. et al. Absolute quantification of the budding yeast transcriptome by means of competitive PCR between genomic and complementary DNAs. *BMC Genomics* **9**, 574 (2008).

53. McShane, E. et al. Kinetic Analysis of Protein Stability Reveals Age-Dependent Degradation. *Cell* **167**, 803–815.e21 (2016).

54. Song, J., Herrmann, J. M. & Becker, T. Quality control of the mitochondrial proteome. *Nat. Rev. Mol. Cell Biol.* 22, https://doi.org/10.1038/s41580-020-00300-2 (2021).

55. Couvillion, M. T., Soto, I. C., Shipkovenska, G. & Churchman, L. S. Synchronized mitochondrial and cytosolic translation programs. *Nature* **533**, 499–503 (2016).

56. Hermann, G. J. et al. Mitochondrial fusion in yeast requires the transmembrane GTPase Fzo1p. *J. Cell Biol.* **143**, 359–373 (1998).

57. Tsuboi, T., Leff, J. & Zid, B. M. Post-transcriptional control of mitochondrial protein composition in changing environmental conditions. *Biochem Soc. Trans.* **48**, 2565–2578 (2020).

58. Lee, S., Lim, W. A. & Thorn, K. S. Improved Blue, Green, and Red Fluorescent Protein Tagging Vectors for S. cerevisiae. *PLoS One* **8**, 4–11 (2013).

59. Goldstein, A. L. & McCusker, J. H. Three new dominant drug resistance cassettes for gene disruption in Saccharomyces cerevisiae. *Yeast* **15**, 1541–1553 (1999).

60. Bertrand, E. et al. Localization of ASH1 mRNA Particles in Living Yeast. *Mol. Cell* **2**, 437–445 (1998).

61. Haim-Vilmovsky, L. & Gerst, J. E. m-TAG: a PCR-based genomic integration method to visualize the localization of specific endogenous mRNAs in vivo in yeast. *Nat. Protoc.* **4**, 1274–1284 (2009).

62. Tinevez, J. Y. et al. TrackMate: An open and extensible platform for single-particle tracking. *Methods*, https://doi.org/10.1016/j.ymeth.2016.09.016 (2017).

63. Rafelski, S. M. et al. Mitochondrial network size scaling in budding yeast. *Science* **338**, 822–824 (2012).

64. Viana, M. P., Lim, S. & Rafelski, S. M. Quantifying Mitochondrial Content in Living Cells. *Methods Cell Biol.* 125 (Elsevier Ltd, 2015).

65. Gillespie, D. T. Stochastic simulation of chemical kinetics. *Annu Rev. Phys. Chem.* **58**, 35–55 (2007).

66. Gillespie, D. T. Exact stochastic simulation of coupled chemical reactions. *J. Phys. Chem.* **81**, 2340–2361 (1977).

67. Viana, M. P. et al. Mitochondrial Fission and Fusion Dynamics Generate Efficient, Robust, and Evenly Distributed Network Topologies in Budding Yeast Cells. *Cell Syst.* **10**, 287–297.e5 (2020).

68. Arceo, X. G., Koslover, E. F., Zid, B. M. & Brown, A. I. Mitochondrial mRNA localization is governed by translation kinetics and spatial transport. *PLoS Comput. Biol.* **18**, e1010413 (2022).

69. Martin-Perez, M. & Villén, J. Determinants and Regulation of Protein Turnover in Yeast. *Cell Syst.* **5**, 283–294.e5 (2017).

70. Sukhorukov, V. M., Dikov, D., Reichert, A. S. & Meyer-Hermann, M. Emergence of the Mitochondrial Reticulum from Fission and Fusion Dynamics. *PLoS Comput. Biol.* **8**, e1002745 (2012).

71. Patel, P. K., Shirihai, O. & Huang, K. C. Optimal Dynamics for Quality Control in Spatially Distributed Mitochondrial Networks. *PLoS Comput. Biol.* **9**, e1003108 (2013).

Author contributions

B.M.Z. and T.T. conceived and designed the project. A.H.K., X.G., and T.T. performed wet experiments and analyzed image data. R.J.P., P.C., A.I.B., and T.T. performed computational experiments and analyzed data. M.P.V., and T.T. developed image processing schemes and methods. A.H.K., A.I.B., B.M.Z., and T.T. wrote the manuscript.

Competing interests

The authors declare no competing interests.

Additional information

Supplementary information The online version contains supplementary material available at https://doi.org/10.1038/s41467-024-52183-y.

Correspondence and requests for materials should be addressed to Brian M. Zid or Tatsuhisa Tsuboi.

Peer review information *Nature Communications* thanks Alistair Green and the other, anonymous, reviewer(s) for their contribution to the peer review of this work. A peer review file is available.

Reprints and permissions information is available at http://www.nature.com/reprints

Publisher's note Springer Nature remains neutral with regard to jurisdictional claims in published maps and institutional affiliations.